

Topological entanglement length in polymer melts and nanocomposites by a DPD polymer model

Cite this: *Soft Matter*, 2013, 9, 3877

Argyrios Karatrantos,^a Nigel Clarke,^{*a} Russell J. Composto^b and Karen I. Winey^b

We investigate the topological constraints (entanglements) in polymer–nanorod nanocomposites in comparison to polymer melts using dissipative particle dynamics (DPD) polymer model simulations. The nanorods have a radius smaller than the polymer radius of gyration and an aspect ratio of 7.5. We observe an increase in the number of entanglements (50% decrease of N_e with 11% volume fraction of nanorods dispersed in the polymer matrix) in the nanocomposites as evidenced by larger contour lengths of the primitive paths. The end-to-end distance is essentially unchanged with the nanorod volume fraction (0–11%). Interaction between polymers and nanorods affects the dispersion of nanorods in the nanocomposites.

Received 16th November 2012

Accepted 11th February 2013

DOI: 10.1039/c3sm27651a

www.rsc.org/softmatter

1 Introduction

The dynamics of long polymers is limited by entanglements, which are topological constraints imposed by the other chains. These can dramatically change the polymer viscosity, mechanical and tribological properties. The addition of nanoparticles to a polymer matrix can result in materials with improved electrical, thermal, mechanical and tribological properties. In this paper we explore how nanoparticles affect rheology by studying the entanglements in polymer–nanoparticle nanocomposites in the case when the polymer radius of gyration ($R_{g,polymer}$) is larger than the nanorod radius (r_{filler}).^{1–5}

Dissipative particle dynamics (DPD) is a mesoscopic simulation method which has become a robust tool for the study of soft matter, including polymer solutions, melts, blends, composites, and surfactants. It was first developed by Hoogerbrugge and Koelman⁶ and reformulated by Groot and Warren.⁷ Later Espanol and Warren⁸ showed that DPD basically consists of particles interacting with a “soft” potential, coupled to a thermostat. The thermostat is not dependent on the “soft” potential.⁹ In many DPD simulations, polymer chains behave as phantom chains,¹⁰ due to the naturally soft interactions between particles (monomeric units), so that they can pass freely through each other and obey Rouse dynamics, over the full range of polymer lengths.

In polymer nanocomposites, the DPD method has been applied to various problems, such as: investigating the role of particle–particle interactions on the viscoelastic behaviour of the nanocomposites,^{11,12} computing the morphology (dispersed

or aggregated nanoparticles) of polymer carbon nanotubes nanocomposites^{13–17} and polymer clay nanocomposites,¹⁸ modelling the self assembly of nanoparticles¹⁹ in a polymer matrix or nanorods in binary blends,^{20,21} and searching the origins of reinforcement.²² To the best of our knowledge, in all of the nanocomposite studies by DPD simulation, the polymer chains behave as phantom chains, thus, quantitative predictions regarding the dynamics, rheological, and mechanical properties in dense entangled melts cannot be extracted.

In recent DPD polymer melt simulation studies different polymer models have been developed to prevent polymer chain crossing, by introducing an additional repulsive interaction which is based on the distance of closest approach between two bonds^{23–28} based on the ideas of Kumar and Larson²⁹ and Pan and Manke,³⁰ or alternatively by introducing an efficient but also computationally demanding algorithm (called the “Twentanglement” algorithm) that detects and prevents unphysical bond crossings^{31,32} by adding a rigid core around monomers,³³ or finally using adaptive timestepping.³⁴ It is still an open question whether the above DPD polymer models can predict, in addition to reptational dynamics³⁵ ($D_0 \approx N^{-2}$, where D_0 is the polymer diffusivity, and N is the number of monomers per chain), the explicit number of monomers between entanglements N_e (the topological entanglement length³⁶) in polymer melts. In this article we use the entangled polymer model for dissipative particle dynamics of Nikunen *et al.*,³⁷ which has already predicted polymer reptational dynamics,³⁵ to investigate the topological entanglement length (which provides a *microscopic* measure of entanglements³⁶), entanglements per chain and primitive path (the shortest path connecting the two ends of the polymer chain subject to the topological constraints) in both polymer melts and nanocomposites by using topological algorithms^{38–41} and applying different entanglements estimators.⁴⁰

^aDepartment of Physics and Astronomy, University of Sheffield, Sheffield S3 7RH, UK. E-mail: n.clarke@sheffield.ac.uk

^bDepartment of Materials Science and Engineering, University of Pennsylvania, Philadelphia, Pennsylvania, 19104, USA

The rest of this paper is organized as follows. In Section II, we present the general features of the simulation methodology and the simulation details that were used to investigate the primitive path of polymers in melts and nanocomposites. Subsequently, in Section III, the theoretical background is given for the entanglement analysis that is implemented in polymer melts and polymer nanocomposites. In Section IV, we discuss the primitive path and entanglements of the DPD polymer melt in comparison to the calculations from molecular dynamics simulations (fully flexible Kremer–Grest model⁴²). In polymer nanocomposites, we investigate the entanglements as a function of polymer molecular weight, volume fraction of filler (nanorods), interaction strength of polymers with fillers (nanorods), and nanorod radius in comparison to theoretical relations. Finally, in Section V, conclusions are presented.

II DPD simulations methodology

The first unique feature of DPD concerns the nature of the conservative force \mathbf{F}_{ij}^C , which is acting along the line between the centres of mass of two particles, and is not a Lennard Jones force^{43,44} (as in molecular dynamics) but decreases linearly with increasing pair distance:

$$\mathbf{F}_{ij}^C = a_{ij} \left(1 - \frac{r_{ij}}{r_c} \right) \mathbf{r}_{ij} \quad (1)$$

where a_{ij} is the maximum repulsion between particle i and particle j (for monomer–monomer repulsion $a = 100^{37}$), r_{ij} represents the distance between particles i and j , and \mathbf{r}_{ij} is the unit vector pointing from particle j to particle i . This simple analytic form results in fast computation per time step, and also can allow a time step orders of magnitude larger than the typical time steps employed in molecular dynamics simulations. During a molecular dynamics simulation, the most time-consuming part is the calculation of the forces due to non-bonded interactions.⁴⁴ Since a “soft” harmonic potential is used (linear conservative force – eqn (1)), the forces cannot be arbitrarily large, thus we can reduce computing times. This soft linear conservative force between particles is deployed in combination with Andersen thermostat⁴⁵ following the idea by Lowe.⁴⁶ The time evolution of the interacting particles is governed by Newton’s equation of motion:

$$\frac{d\mathbf{r}_i}{dt} = \mathbf{v}_i \quad (2)$$

$$\frac{d\mathbf{v}_i}{dt} = \mathbf{f}_i \quad (3)$$

The total force on particle i , \mathbf{f}_i , is given by the sum of two terms, each due to the pairwise additive interactions with other particles in the system.

$$\mathbf{f}_i = \sum_{i \neq j} \left(\mathbf{F}_{ij}^C + \mathbf{F}_{ij}^S \right) \quad (4)$$

All these forces are taken to be zero beyond a certain cut off radius $r_c = 1$. Also, the monomers were connected using harmonic springs:

Table 1 Results for the computational efficiency of the potential used in a polymer melt simulation ($N = 200$, $N_p = 300$). The WCA potential⁵⁶ was used in the MD simulation (fully flexible Kremer–Grest (bead-spring) model,⁴² $r_c = 2^{1/6}\sigma$, $\sigma = 1$). (Single core CPU type used: AMD 2218HE, MD simulations performed using GROMACS^{57–60})

Model-potential	Density (ρ)	Steps	dt (τ)	CPU time (sec)
DPD: soft – eqn (1)	1	10^5	0.01	0.02375
DPD: soft – eqn (1)	1	2×10^5	0.005	0.024375
Bead-spring: WCA	0.85	10^5	0.01	0.04714
Bead-spring: WCA	0.85	2×10^5	0.005	0.047265

$$\mathbf{F}_i^S = \sum_j k(r_0 - r_{ij}) \quad (5)$$

where the sum is over all particles j to which particle i is connected. The equilibrium bond length was set to $r_0 = 0.95$, and $k = 200$.³⁷

Simulations details

The simulations were performed at a monomer density $\rho = (N_m/V) = 1$ (where N_m is the total number of monomeric units in the system and V is the volume of the system). The length of the simulation cell was always larger than the end-to-end distance of the polymer chains. To set the temperature at $T^* = k_B T/\epsilon = 1$, the Andersen thermostat⁴⁵ was used. The equations of motion were integrated using the velocity Verlet algorithm with a time step equal to 0.02τ , where $\tau = (mr_c^2/k_B T)^{1/2}$ is the time unit, and $m = 1$. In MD simulations the Lennard Jones potential used enforces a smaller time step. In all the previous studies of polymer melts with MD simulations and a DPD^{9,47–51} or Langevin^{52–55} thermostat, the time step used ($dt = 0.005–0.012\tau$) used was smaller than that in our work. All the systems were started from random flight initial configurations, and equilibrated for 10^7 , 5×10^5 , 1.5×10^5 time steps for $N = 200$, $N = 75$, 100 and $N = 10$, 20, 25, 40 respectively. The same methodology of equilibration has been reported previously.³⁷ The duration of the simulation runs were between 2.5 and 20×10^6 steps depending on the length of molecules. The simulations run long enough such that the polymer chains (for $N = 200$, at $\phi = 11\%$) moved approximately $2R_g$ distance. Details (number of polymers N_p , number of monomers N in a polymer chain, length of the cubic simulation cell L , end-to-end vector distance, primitive path dimensions as calculated from the Z1 topological algorithm^{38–41}) of the polymer melt simulated systems are given in Table 2. Also in order to have an idea of the computational efficiency of the “soft” harmonic potential used in our work we calculated the CPU time needed for a single time step dt . We present the CPU time in Table 1.

III Estimators for topological entanglement length N_e

In polymer melts of sufficiently long flexible chain molecules, neighbouring chains strongly interpenetrate and entangle with each other.³⁵ The motion of the polymers is dominated by the restriction that chains may slide past but not through each

other. Thus, the motion of polymers whose degree of polymerization becomes larger than the “entanglement length” N_e is confined to a tubelike region.

Let us now discuss N_e as determined by the estimator of Everaers *et al.*⁶¹ (which we denote as classical S-coil), evaluated using the geometrical Z1 algorithm.^{38–41} This N_e estimator is determined by statistical properties of the primitive path as a whole coil and evaluated for a given N as follows:

$$\mathcal{A}_e(N) = (N - 1) \frac{\langle R_{ee}^2 \rangle}{\langle L_{pp} \rangle^2} \quad (6)$$

where R_{ee} is the end-to-end vector distance of a polymer chain and L_{pp} is the contour length of its primitive path, the averages are taken over the ensemble of chains.

Another estimator for the entanglement length can be used by measuring the number of interior “kinks”^{38,39} which is considered to be proportional to the number of entanglements. The estimator on the number of kinks, $\langle Z \rangle$ is denoted here as classical S-kink is given by:³⁸

$$\mathcal{A}_e(N) = \frac{N(N - 1)}{Z(N - 1) + N} \quad (7)$$

Differences between the Z1 algorithm and the primitive path analysis^{52,61} and the difference between N_e estimated from kinks and coils has been discussed previously.^{39,40} It is known that using the classical S-coil and S-kink estimators eqn (6) following⁶¹ one underestimates N_e . However, it is known that $N_e \equiv \lim_{N \rightarrow \infty} \mathcal{A}_e(N)$ (N -independent quantity).

In addition, there are modified estimators that provide an upper bound for N_e , such as the modified S-coil,⁴⁰ but they tend to overestimate N_e for weakly entangled chains:

$$\mathcal{A}_e(N) = (N - 1) \left(\frac{\langle L_{pp}^2 \rangle}{\langle R_e^2 \rangle} - 1 \right)^{-1} \quad (8)$$

However, in all these single chain estimators for the N_e , the non-Gaussian statistics of chains and primitive paths produce systematic errors.⁴⁰ In order to eliminate the systematic errors that appear in the previous estimators and to obtain an accurate N -independent value, we use an ideal N_e estimator (M-coil),⁴⁰ which requires simulation of multiple chain lengths, using coil properties:

$$\left(\frac{C(x)}{x} \right)_{x=\mathcal{A}_e(N)} = \frac{d}{dN} \left(\frac{\langle L_{pp}^2 \rangle}{R_{RW}^2(N)} \right) \quad (9)$$

where $C(x) \equiv \langle R_{ee}^2 \rangle / R_{RW}^2(x)$ is the characteristic ratio⁶² for a chain with x monomers, and $R_{RW}^2(x) = (x - 1)r_0^2$ is the reference mean squared end-to-end distance of a random walk. The derivative of eqn (9) means that the $\langle L_{pp} \rangle$ needs to be measured as function of N .

The averages in our analysis are taken over the ensemble of all chains at each time step. Then the time average is taken for 250 saved configurations (at a time larger than the disentanglement time, ($t > \tau_e$), in which the polymer chains have diffused at least an end-to-end distance). In order to obtain an error bar for the N_e values in eqn (9), we solve the M-coil estimator again

Table 2 Number of polymers in the simulation cell (N_p), monomers in a polymer chain (N), length of the simulation cell (L), square end-to-end vector distance ($\langle R_{ee}^2 \rangle$), L_{pp} , $\langle L_{pp}^2 \rangle$, number of kinks (Z) for polymer melt systems studied in the present simulations

N_p	N	L	R_{ee}^2	L_{pp}	L_{pp}^2	Z
576	10	17.926	11.587	3.257	11.975	0.018
4000	15	39.148	18.914	4.201	20.041	0.049
3000	20	39.148	26.329	5.056	29.178	0.126
2400	25	39.148	33.757	5.851	39.152	0.224
2000	30	39.148	41.311	6.624	50.167	0.338
1024	50	37.133	75.971	9.543	105.16	0.837
1000	60	39.148	87.1	10.96	135.494	1.068
800	75	26.777	111.207	13.084	191.991	1.444
288	80	28.455	116.905	13.614	207.798	1.531
665	90	28.455	133.377	15.058	252.838	1.773
512	100	37.133	148.421	16.406	298.608	1.994
512	128	40.317	192.47	20.052	441.958	2.554
384	150	38.619	222.929	23.061	578.9	3.033
300	200	39.148	299.523	29.845	957.981	4.086

for the lower and upper limits of R_{ee} (end-to-end vector distance) and L_{pp} (contour length of primitive path) as these are extracted from the Z1 algorithm.^{38–41}

IV Results and discussion

A Polymer melt

The chain and primitive path dimensions as calculated from the Z1 algorithm^{38–41} for the polymer melts studied are presented in Table 2. We depict the behaviour of modified S-coil, classical S-coil, and classical S-kink (eqn (6), (8), and (7), respectively) for the DPD entangled polymer model³⁷ in Fig. 1 in comparison with the molecular dynamics simulations⁴⁰ of the fully flexible Kremer–Grest model.⁴² Very good agreement is found between the DPD polymer melt data and the molecular dynamics data. The upper and lower bounds of N_e for the

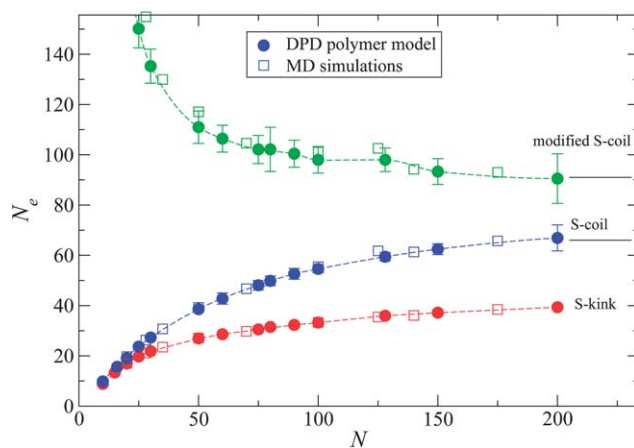


Fig. 1 DPD polymer model simulations yield N_e estimated from $\mathcal{A}_e(N)$ using eqn (6) (blue), eqn (8) (green), and eqn (7) (red) for polymer melts. Dashed lines interpolating between filled data points have been added to guide the eye. For comparison, MD simulations⁴⁰ of fully flexible Kremer–Grest model⁴² (squares) are included.

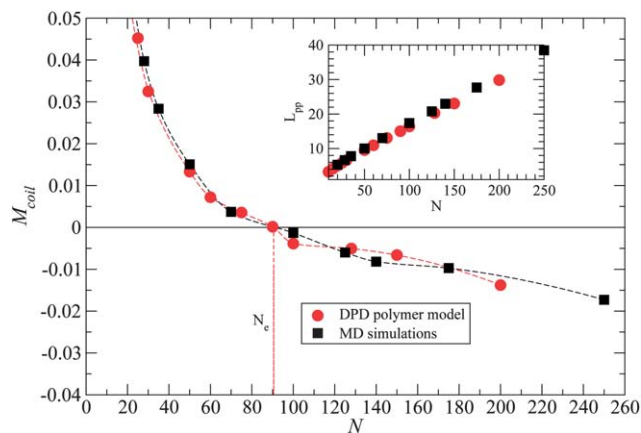


Fig. 2 DPD polymer model simulations yield N_e estimated from $\mathcal{N}_e(N)$ using the M-coil estimator (eqn (9)) for polymer melts. Dashed lines interpolating between data points have been added to guide the eye. Inset: contour length of the primitive path L_{pp} for different number of monomers per chain, N . For comparison, MD simulations⁴⁰ of fully flexible Kremer–Grest model⁴² (squares) are included.

polymer melt are 91 and 66, respectively, as shown by the black lines in Fig. 1.

In Fig. 2, we depict the M-coil estimator eqn (2) for the DPD polymer model. Again there is very good agreement (also, for the contour length of the primitive path L_{pp} : inset of Fig. 2) with the calculations from molecular dynamics simulations⁴⁰ for the fully flexible Kremer–Grest model.⁴² From Fig. 2, it can be extracted that $N_e \approx 90.52$ (with a lower limit: 87.6 and upper limit 92), which coincides with that of Kremer–Grest model. Also, $N_e \in [66, 91]$ from the S-coils, which is comparable with previous studies that found $N_e \approx 85$ ^{40,63} (for the fully flexible

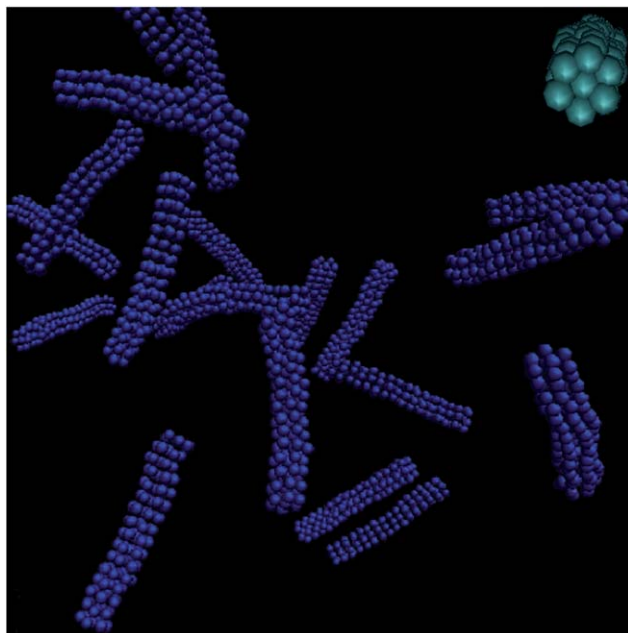


Fig. 3 Snapshot of hexagonal nanorods. Polymer chains are not shown. Inset: cross-section of the nanorod used in this work.

Table 3 Nanorod volume fraction (%), number of nanorods N_{rod} , bond length of nanorod atoms r_0 (force constant is set to $k = 400$), average diameter of nanorods D_{rod} , for nanocomposite systems studied in the present simulations. Aspect ratio of nanorods: $L/D \approx 7.5$. Nonbonded interactions, according to eqn (1), are considered between all atom pairs

Volume%	N_{rod}	
	$r_0 = 0.7, D_{rod} = 1.52$	$r_0 = 0.8, D_{rod} = 1.68$
0.6875	24	18
2.75	96	72
5.5	192	144
11	384	288

Kremer–Grest model⁴²). The error bar is of the order of 3%, thus our simulations performed in this study can predict a reliable N_e value. The excellent agreement between our DPD and the MD simulations may be coincidental given the difference in monomer density.

B Nanocomposites

For nanocomposites, we consider systems of hexagonal nanorods (see Fig. 3 and its inset: cross-section of nanorods has an hcc structure) in a dense polymer melt of entangled polymers. In all of the systems studied, a total number of $N_t = 60\,000$ monomers were used in a cubic box, increasing the length of the simulation cell L according to the volume fraction of the nanorods in order to have a monomer density $\rho = 1$; this maintains a constant free volume in the polymer melt. The polymer–nanorod interaction is set to $a_{ij} = 25$. Details of the nanocomposite systems studied (volume fraction, number, nanorod bond distance, and diameter of nanorods) are summarized in Table 3. In such systems we consider the case of the primitive path analysis for both the frozen particle limit,

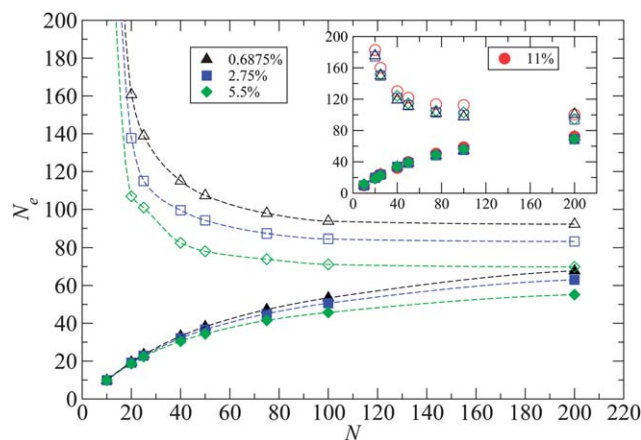


Fig. 4 N_e estimated from $\mathcal{N}_e(N)$ using eqn (6) (filled symbols) and eqn (8) (open symbols) for polymer–nanorod nanocomposites. (i) 0.6875% (black triangles), (ii) 2.75% (blue squares), (iii) 5.5% (green diamonds). Dashed lines interpolating between data points have been added to guide the eye. The same trends are followed for 11% volume fraction (results not shown for clarity). Inset: N_e estimation, where prior to the primitive path analysis the nanorods are removed (replaced with vacancies).

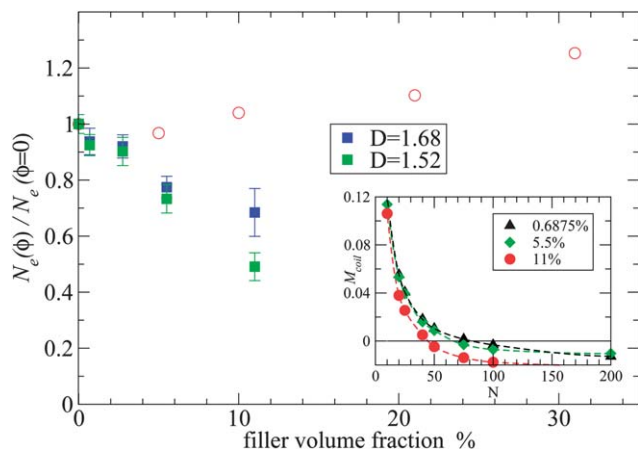


Fig. 5 Dependence of $N_e(\phi)/N_e(\phi=0)$ ratio with filler volume fraction in nanocomposites for different fillers: (i) DPD simulations with nanorod ($D = 1.52$) fillers (green symbols), (ii) DPD simulations with nanorod ($D = 1.68$) fillers (blue symbols), (iii) MD simulations with spherical fillers (open symbols).⁷⁴ Inset: N_e estimated from $M_{\text{coil}}(N)$ using the M-coil estimator (eqn (9)) for polymer nanocomposites ($D = 1.52$) from DPD simulations: (i) 0.6875% (black triangles), (ii) 5.5% (green diamonds), (iii) 11% (red circles). Dashed lines interpolating between data points have been added to guide the eye. The same trend is followed for 2.75% volume fraction (results not shown for clarity).

where nanoparticles with fixed coordinates are explicitly in the entanglement analysis, and phantom particle limit where nanoparticles are replaced with vacancies prior to the entanglement analysis.

1 Effect of volume fraction. Similar to the polymer melt, the S-coil estimators are used for each nanocomposite system studied and their predictions are depicted in Fig. 4. It clearly shows the effect of the volume fraction on the behaviour of the N_e : the addition of nanorods decreases the N_e from the modified S-coil and increases N_e from the classical S-coil. Moreover, in the phantom particle limit, the volume fraction of nanorods

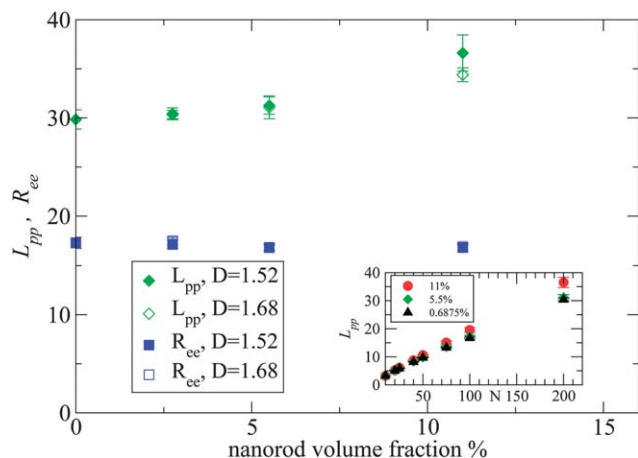


Fig. 6 Contour length of primitive path L_{pp} (diamonds) and end-to-end distance R_{ee} (squares) ($N = 200$) in nanocomposites for different nanorod volume fractions. Inset: contour length of the primitive path L_{pp} ($D = 1.52$) for different number of monomers per chain, N : (i) 0.6875% (black triangles), (ii) 5.5% (green diamonds), (iii) 11% (red circles).

does not really alter N_e for the volume fractions studied, as can be seen in the inset of Fig. 4. In addition, the M-coil estimator of N_e is used for each nanocomposite system in order to have an N -independent estimation of N_e , and is depicted in the inset of Fig. 5. Clearly, increasing volume fraction of nanorods reduces N_e and also L_{pp} increases, as can be seen in the Fig. 6.

The concept of entanglement length is useful because it relates changes in structure to rheological properties.^{52,61,64} For polymer melts, a temperature and concentration dependent material constant, the plateau shear modulus G_N^0 , which is of the order of 10^6 Pa, or five orders of magnitude smaller than the shear modulus of the ordinary solids, is related to N_e by eqn (10).^{52,61,65,66}

$$G_N^0 = \frac{4 \rho k_B T}{5 N_e^{\text{rheo}}} \quad (10)$$

where, ρ is the monomer density, N_e^{rheo} is the rheological entanglement length.³⁶ G_N^0 is also inversely proportional to p^3 , where p is the packing length, a characteristic length scale at which polymers start to interpenetrate.

In polymer nanocomposites the validity of eqn (10) is unclear, however, a dependence of the plateau modulus $G_N^0(\Phi) = G_N^0(\Phi = 0) \times f(\Phi)$ on the filler degree Φ has been observed for repulsive systems with $R_{g,\text{polymer}} > r_{\text{filler}}$ (such as PEP-POSS, PI-POSS).^{67–69}

$$f(\Phi) = 1 + [\eta]\beta\Phi + a_2(\beta\Phi)^2 + a_3(\beta\Phi)^3 + \dots \quad (11)$$

where, $\eta = 2.5$,^{70,71} $a_2 = 14.1$,⁷² and β is an effectiveness factor.⁷³ The ratio of $N_e(\phi)/N_e(\phi = 0)$, in our simulations, decreases with the nanorod volume fraction, specifically at 11% volume fraction the ratio decreases 50%.

The addition of nanorods in the polymer melt decreases the N_e value, thus the “predicted” plateau shear modulus G_N^0 increases since it is inverse proportional to N_e^{rheo} ($N_e^{\text{rheo}} = 2N_e$ for loosely entangled polymer chains).³⁶ For low volume fraction of nanorods the zero shear viscosity ratio is analogous to that of the plateau shear modulus ($\eta_0(\phi)/\eta_0(\phi = 0) = G_N^0(\phi)/G_N^0(\phi = 0)$), thus it will be increased by the addition of nanoparticles. Moreover, the polymer chain dynamics is also affected by the filler volume fraction. Since by increasing the number of nanorods and retaining the same free volume in the nanocomposite systems there are more topological constraints created, the polymer chain dynamics is hindered.

Instead, in nanocomposites systems with repulsive spherical nanoparticles⁷⁴ in which $R_{g,\text{polymer}} \approx r_{\text{filler}}$, the N_e increases with the volume fraction of the nanoparticles due to the decrease of the L_{pp} . As a result, the entangled polymer chains gradually disentangle upon the addition of the spherical nanoparticles.⁷⁴ However in nanocomposites systems with attractive spherical nanoparticles⁷⁵ of same size to⁷⁴ the N_e does not change from the bulk value, at least in the case of $\phi = 11\%$.

2 Effect of nanorod radius. Increasing the radius of the nanorods at a constant nanorod length and volume fraction decreases the surface area to volume ratio of the nanorods, and there is a larger depletion layer formed around the nanorods' surface.^{3,4} The effect of the nanorod radius on the

$N_e(\phi)/N_e(\phi = 0)$ ratio from the DPD simulations is depicted in Fig. 5. As can be seen, for the larger radius, the ratio is slightly higher. Also we calculated the entanglements in the phantom particle limit and found that the polymer–polymer path network is not altered (N_e is independent on the nanorod radius and nanorod volume fraction according to the inset of Fig. 4), which is in agreement with molecular dynamics data.⁷⁶ The dimensions of R_{ee} and L_{pp} , for polymers of $N = 200$, as a function of the volume fraction of the nanorods are shown in Fig. 6. It can be seen that R_{ee} is essentially unchanged, in comparison to its melt value and independent on nanotube radius, with the volume fraction of nanorods in this system with non-attractive

nanorods. This contrasts with previous studies for attractive spherical nanoparticles^{77,78} where there is an increase up to 15% in polymer dimensions. However, L_{pp} increases with the addition of nanorods due to more topological constraints being created.

Furthermore, a disentanglement effect does not appear in the vicinity of nanorod, as was recently reported, for thin polymer films,⁷⁹ on a bare flat surface⁸⁰ and on large spherical nanoparticles.⁷⁴ The disentanglement effect in such systems is due to the fact that polymers in the vicinity of the surface only have neighbouring chains on one side and no chains to entangle with on the other side, thus they have a smaller total number of entanglements.

3 Effect of polymer–nanorod interaction strength. By tuning the polymer–nanorod interaction a_{ij} of eqn (1), the dispersion and aggregation behaviour (which takes place in polymer–SWCNT nanocomposites⁸¹) and mechanisms of the nanorods in nanocomposites can be explored. While these mechanisms have been studied in nanocomposites with spherical nanoparticles, by molecular dynamics simulation,⁸² its effect on the entanglements has not been investigated. In addition, the investigation of such mechanisms by molecular dynamics presents limitations such as finite size effects, simulations of only weakly entangled polymers, equilibration time, which can be overcome by the implementation of DPD simulations.

By increasing the a_{ij} parameter we were able to produce systems with an increased degree of nanorod–nanorod aggregation. Thus a_{ij} can alter the morphology of the nanorods in the polymer melt as can be seen in Fig. 7.

V Conclusions

The topological constraints of polymers in melts and nanocomposites with nanorods were investigated using a DPD polymer model. We applied different estimators $\mathcal{N}_e(N)$ and extracted the N -independent topological entanglement length N_e . We found that the DPD polymer model used can describe N_e accurately in comparison to molecular dynamics simulations of the fully flexible Kremer–Grest model. We investigated polymer nanocomposites for the first time using an entangled DPD polymer model. We observe that the entanglement length decreases significantly with volume fraction of hexagonal nanorods. This decrease of N_e in the polymer melt with nanorods originates from the polymer/nanorod entanglements, because the contour length of the primitive path, L_{pp} , increases with the addition of nanorods, while the R_{ee} is essentially unchanged in comparison to its value in polymer melts. Finally, the polymer–nanorod interaction alters the morphology of the nanocomposites.

Acknowledgements

We thank Prof. [M. Kröger](#) for providing us the Z1 algorithm. This research was funded by the EPSRC/NSF Materials Network program EP/5065373/1 (EPSRC: NC, AK) and DMR-0908449 (NSF: KIW, RJC).

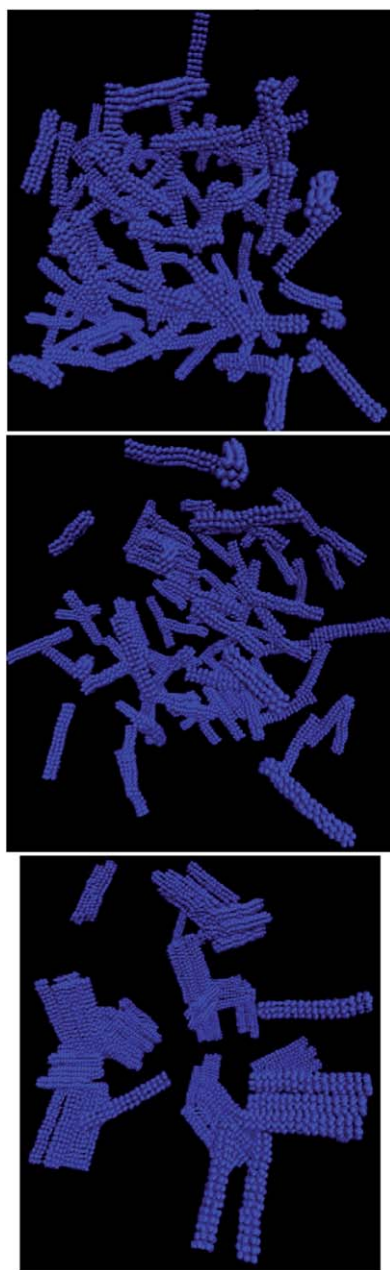


Fig. 7 Nanorod morphology for different polymers–nanorod interaction strength at 2.75% volume fraction (from top to bottom $a_{ij} = 25, 50, 75$). Polymer chains are not shown.

References

- 1 M. Mu, R. J. Composto, N. Clarke and K. I. Winey, *Macromolecules*, 2009, **42**, 8365.
- 2 M. Mu, N. Clarke, R. J. Composto and K. I. Winey, *Macromolecules*, 2009, **42**, 7091.
- 3 A. Karatrantos and N. Clarke, *Soft Matter*, 2011, **7**, 7334.
- 4 A. Karatrantos, R. J. Composto, K. I. Winey and N. Clarke, *Macromolecules*, 2011, **44**, 9830.
- 5 A. Karatrantos, R. J. Composto, K. I. Winey, M. Kröger and N. Clarke, *Macromolecules*, 2012, **45**, 7274.
- 6 P. J. Hoogerbrugge and J. M. V. A. Koelman, *Europhys. Lett.*, 1992, **19**, 155.
- 7 R. D. Groot and P. B. Warren, *J. Chem. Phys.*, 1997, **107**, 4423.
- 8 P. Espanol and P. Warren, *Europhys. Lett.*, 1995, **30**, 191.
- 9 T. Soddemann, B. Dünweg and K. Kremer, *Phys. Rev. E: Stat. Phys., Plasmas, Fluids, Relat. Interdiscip. Top.*, 2003, **68**, 046702.
- 10 N. A. Spenley, *Europhys. Lett.*, 2000, **49**, 534.
- 11 G. Raos, M. Moreno and S. Elli, *Macromolecules*, 2006, **39**, 6744.
- 12 V. Pryamitsyn and V. Ganesan, *Macromolecules*, 2006, **39**, 844.
- 13 A. Maiti, J. Wescott and P. Kung, *Mol. Simul.*, 2005, **31**, 143.
- 14 A. Maiti, *Microelectron. J.*, 2008, **39**, 208.
- 15 M. Ionita, I. V. Branzoi and L. Pilan, *Surf. Interface Anal.*, 2010, **42**, 987.
- 16 Y. C. Wang, S. P. Ju, J. Z. Cheng, J. M. Lu and H. H. Wang, *J. Phys. Chem. C*, 2010, **114**, 3376.
- 17 Y. C. Wang, S. P. Ju, T. J. Huang and H. H. Wang, *Nanoscale Res. Lett.*, 2011, **6**, 433.
- 18 G. Scocchi, P. Posocco, A. Danani, S. Pricl and M. Fermeglia, *Fluid Phase Equilib.*, 2007, **261**, 366.
- 19 S. W. Hu, Y. J. Sheng and H. K. Tsao, *J. Phys. Chem. C*, 2012, **116**, 1789.
- 20 M. J. A. Hore and M. Laradji, *J. Chem. Phys.*, 2008, **128**, 054901.
- 21 L. T. Yan, E. Maresov, G. A. Buxton and A. C. Balazs, *Soft Matter*, 2011, **7**, 595.
- 22 G. Raos and M. Casalegno, *J. Chem. Phys.*, 2011, **134**, 054902.
- 23 S. P. Holleran and R. G. Larson, *Rheol. Acta*, 2008, **47**, 3.
- 24 F. Lahmar, C. Tzoumanekas, D. N. Theodorou and B. Rousseau, *Macromolecules*, 2009, **42**, 7474.
- 25 F. Goujon, P. Malfreyt and D. J. Tildesley, *J. Chem. Phys.*, 2008, **129**, 034902.
- 26 F. Goujon, P. Malfreyt and D. J. Tildesley, *Macromolecules*, 2009, **42**, 4310.
- 27 M. Yamanoi, O. Pozo and J. M. Maia, *J. Chem. Phys.*, 2011, **135**, 044904.
- 28 T. W. Sirk, Y. R. Sliozberg, J. K. Brennan, M. Lisal and J. W. Andzelm, *J. Chem. Phys.*, 2012, **136**, 134903.
- 29 S. Kumar and R. G. Larson, *J. Chem. Phys.*, 2001, **114**, 6937.
- 30 G. Pan and C. W. Manke, *Int. J. Mod. Phys. B*, 2003, **17**, 231.
- 31 J. T. Padding and W. J. Briels, *J. Chem. Phys.*, 2003, **118**, 10276.
- 32 T. Padding and W. J. Briels, *J. Chem. Phys.*, 2001, **115**, 2846.
- 33 H. Liu, Y. H. Xue, H. J. Qian, Z. Y. Lu and C. C. Sun, *J. Chem. Phys.*, 2008, **129**, 024902.
- 34 N. Hoda and R. G. Larson, *J. Rheol.*, 2010, **54**, 1061.
- 35 M. Doi and S. F. Edwards, *The Theory of Polymer Dynamics*, Clarendon Press, Oxford, 1986.
- 36 R. Everaers, *Phys. Rev. E: Stat., Nonlinear, Soft Matter Phys.*, 2012, **86**, 022801.
- 37 P. Nikunen, M. Karttunen and I. Vattulainen, *Phys. Rev. E: Stat., Nonlinear, Soft Matter Phys.*, 2007, **75**, 036713.
- 38 M. Kröger, *Comput. Phys. Commun.*, 2005, **168**, 209.
- 39 S. Shanbhag and M. Kröger, *Macromolecules*, 2007, **40**, 2897.
- 40 R. S. Hoy, K. Foteinopoulou and M. Kröger, *Phys. Rev. E: Stat., Nonlinear, Soft Matter Phys.*, 2009, **80**, 031803.
- 41 N. C. Karayiannis and M. Kröger, *Int. J. Mol. Sci.*, 2009, **10**, 5054.
- 42 K. Kremer and G. S. Grest, *J. Chem. Phys.*, 1990, **92**, 5057.
- 43 M. P. Allen and D. J. Tildesley, *Computer Simulation of Liquids*, Clarendon Press, Oxford, 1987.
- 44 B. Frenkel, and D. Smit, *Understanding Molecular Simulation: From Algorithms to Applications (Computational Science)*, Academic Press, 1996.
- 45 H. Andersen, *J. Chem. Phys.*, 1980, **72**, 2384.
- 46 Lowe, *Europhys. Lett.*, 1999, **47**, 145.
- 47 S. Peter, H. Meyer and J. Baschnagel, *Eur. Phys. J. E*, 2009, **28**, 147.
- 48 J. Farago, H. Meyer and A. N. Semenov, *Phys. Rev. Lett.*, 2011, **107**, 178301.
- 49 J. Farago, H. Meyer, J. Baschnagel and A. N. Semenov, *J. Phys.: Condens. Matter*, 2012, **24**, 284105.
- 50 M. Durand, H. Meyer, O. Benzerara, J. Baschnagel and O. Vitrac, *J. Chem. Phys.*, 2010, **132**, 194902.
- 51 D. Reith, A. Milchev, P. Virnau and K. Binder, *Macromolecules*, 2012, **45**, 4381.
- 52 S. K. Sukumaran, G. S. Grest, K. Kremer and R. Everaers, *J. Polym. Sci., Part B: Polym. Phys.*, 2005, **43**, 917.
- 53 M. Putz, K. Kremer and G. S. Grest, *Europhys. Lett.*, 2000, **49**, 735.
- 54 R. Auhl, R. Everaers, G. S. Grest, K. Kremer and S. J. Plimpton, *J. Chem. Phys.*, 2003, **119**, 12718.
- 55 J. D. Halverson, W. B. Lee, G. S. Grest, A. Y. Grosberg and K. Kremer, *J. Chem. Phys.*, 2011, **134**, 204904.
- 56 J. D. Weeks, D. Chandler and H. C. Andersen, *J. Chem. Phys.*, 1971, **24**, 5237.
- 57 H. Bekker, H. J. C. Berendsen, E. J. Dijkstra, S. Achterop, R. van Drunen, D. van der Spoel, A. Sijbers, H. Keegstra, B. Reitsma, and M. K. R. Renardus, *Physics Computing*, 1993, vol. 92, p. 252.
- 58 H. J. C. Berendsen, D. van der Spoel and R. van Drunen, *Comput. Phys. Commun.*, 1995, **91**, 43.
- 59 E. Lindahl, B. Hess and D. van der Spoel, *J. Mol. Model*, 2001, **7**, 306.
- 60 D. van der Spoel, E. Lindahl, B. Hess, G. Groenhof, A. Mark and H. Berendsen, *J. Comput. Chem.*, 2005, **26**, 1701.
- 61 R. Everaers, S. K. Sukumaran, G. S. Grest, C. Svaneborg, A. Sivasubramanian and K. Kremer, *Science*, 2004, **303**, 823.
- 62 P. Flory, *Statistical Mechanics of Chain Molecules*, Hanser, Munchen, 1989.
- 63 J. X. Hou, C. Svaneborg, R. Everaers and G. S. Grest, *Phys. Rev. Lett.*, 2010, **105**, 068301.

- 64 N. Uchida, G. S. Grest and R. Everaers, *J. Chem. Phys.*, 2008, **128**, 044902.
- 65 K. Kremer, S. K. Sukumaran, R. Everaers and G. S. Grest, *Comput. Phys. Commun.*, 2005, **169**, 75.
- 66 R. H. Colby, M. Rubinstein and J. L. Viovy, *Macromolecules*, 1992, **25**, 996.
- 67 H. Eggers and P. Schuemmer, *Rubber Chem. Technol.*, 1996, **69**, 253.
- 68 G. Heinrich, M. Kluppel and T. A. Vilgis, *Curr. Opin. Solid State Mater. Sci.*, 2002, **6**, 195.
- 69 E. T. Kopesky, T. S. Haddad, G. H. McKinley and R. E. Cohen, *Polymer*, 2005, **46**, 4743.
- 70 A. Einstein, *Ann. Phys.*, 1906, **19**, 289.
- 71 H. J. Smallwood, *J. Appl. Phys.*, 1944, **15**, 758.
- 72 E. Guth and O. Gold, *Phys. Rev.*, 1938, **53**, 322.
- 73 K. Nusser, G. I. Schneider, W. Pyckhout-Hintzen and D. Richter, *Macromolecules*, 2011, **44**, 7820.
- 74 Y. Li, M. Kröger and W. K. Liu, *Phys. Rev. Lett.*, 2012, **109**, 118001.
- 75 J. T. Kalathi, G. S. Grest and S. K. Kumar, *Phys. Rev. Lett.*, 2012, **109**, 198301.
- 76 G. N. Toepperwein, N. C. Karayiannis, R. A. Riggleman, M. Kröger and J. J. de Pablo, *Macromolecules*, 2011, **44**, 1034.
- 77 A. L. Frischknecht, E. S. McGarrity and M. E. Mackay, *J. Chem. Phys.*, 2010, **132**, 204901.
- 78 M. Goswami and B. G. Sumpter, *Phys. Rev. E: Stat., Nonlinear, Soft Matter Phys.*, 2010, **81**, 041801.
- 79 H. Meyer, T. Kreer, A. Cavallo, J. P. Wittmer and J. Baschnagel, *Eur. Phys. J.: Spec. Top.*, 2007, **141**, 167.
- 80 M. Vladkov and J. L. Barrat, *Macromolecules*, 2007, **40**, 3797.
- 81 M. Moniruzzaman and K. I. Winey, *Macromolecules*, 2006, **39**, 5194.
- 82 J. Liu, Y. Gao, D. Cao, L. Zhang and Z. Guo, *Langmuir*, 2011, **27**, 7926.